Mechanistic basis of temperature-dependent dwell fatigue in titanium alloys

Zebang Zheng [*,a], Daniel S. Balint [b], Fionn P.E. Dunne [a, b]

[a] Department of Materials, Imperial College London, London SW7 2AZ, United Kingdom
[b] Department of Mechanical Engineering, Imperial College London, London SW7 2AZ, United Kingdom

Abstract

The temperature-dependent dwell sensitivity of Ti-6242 and Ti-6246 alloys has been assessed over a temperature range from $-50℃$ to $390℃$ using discrete dislocation plasticity which incorporates both thermal activation of dislocation escape from obstacles and slip transfer across grain boundaries. The worst-case load shedding in Ti-6242 alloy is found to be at or close to $120℃$ under dwell fatigue loading, which diminishes and vanishes at temperatures lower than $-50℃$ or higher than $230℃$. Load shedding behaviour is predicted to occur in alloy Ti-6246 also but over a range of higher temperatures which are outside those relevant to in-service conditions. The key controlling dislocation mechanism with respect to load shedding in titanium alloys, and its temperature sensitivity, is shown to be the time constant associated with the thermal activation of dislocation escape from obstacles, with respect to the stress dwell time. The mechanistic basis of load shedding and dwell sensitivity in dwell fatigue loading is presented and discussed in the context of experimental observations.

Keywords: Cold dwell fatigue; Temperature sensitivity; Discrete dislocation plasticity; Hexagonal close-packed; Load shedding

[*] *Corresponding author: zebang.zheng12@imperial.ac.uk*

1. Introduction

The study of dwell sensitivity in titanium alloys can be traced back to the early 1970s when cold dwell fatigue was first detected in Rolls-Royce RB211 engines on Lockheed Tristar aircraft (Bache, 2003). The dwell fatigue loading cycle can be represented for a single duty cycle of a gas turbine engine (Bache, 2003) as shown in Fig. 1. Despite the long (cruise) stress dwell shown, the most damaging part of the loading history is thought to be quite early in the cycle close to peak load achievement. Under the low-cycle dwell fatigue tests, where each loading cycle consists of a stress hold period at the maximum stress, near-α titanium alloys have been reported to display significant lifetime reduction in comparison to low-cycle fatigue tests. Dunne et al. (2007a) and Zheng et al. (2016a) have demonstrated that stress-controlled dwell fatigue loading causes higher damage compare to loading with a strain hold. The lifetime reduction has been called 'cold dwell debit' because its magnitude is maximized at low temperatures, e.g. $\sim 0.4T_m$ where T_m is the absolute melting point. The formation of facet micro-cracking on basal slip planes of hexagonal close-packed crystals (HCP) is argued to cause the early nucleation of defects hence leading to a short lifetime under dwell fatigue loading (Bache, 2003; Evans and Bache, 1994; Lütjering and Williams, 2003; Sinha et al., 2006). The nucleation of faceting has been reported to be highly related to the strong anisotropy of the HCP structure and always associated with a particular crystallographic orientation combination: a soft grain (well-orientated for slip) sits adjacent to a hard grain (c-axis parallel to the loading), sometimes known as a *rogue* grain combination (Anahid et al., 2011; Dunne, 2014; Dunne and Rugg, 2008; Dunne et al., 2007b; Kirane et al., 2009; Sinha et al., 2006).

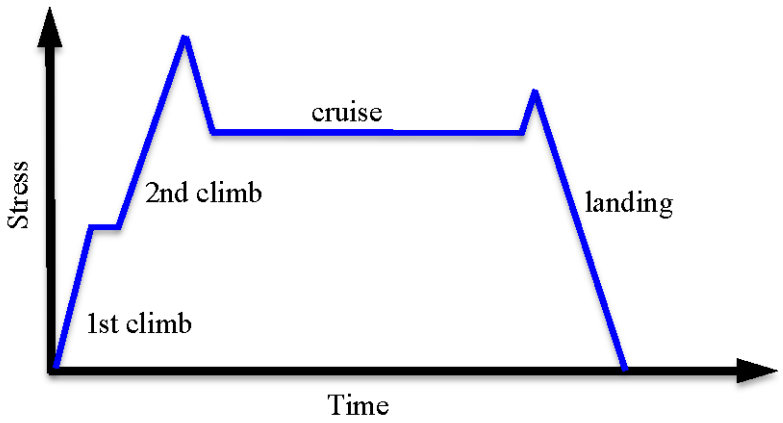


Fig. 1. Schematic diagram of a single duty cycle for a gas turbine engine (Bache, 2003).

The near-room temperature creep behaviour of near-α Ti alloys is argued to be responsible for their dwell sensitivities. Hasija et al. (2003) examined the creep of Ti-6Al alloy and found that it led to the redistribution of stress from the soft grain to the adjacent hard grain, termed load shedding, under dwell fatigue loading, and argued that this contributed to local crack initiation. Stroh (1954) established an analytical model to calculate the stress developed by a dislocation pileup along a line of slip in an elastic medium, from which a crack nucleation criterion was derived. This model was recently developed further to include alternative loading stress states and validated using discrete dislocation plasticity (DDP) modelling to

understand the dwell fatigue behaviour of Ti-6Al alloy (Zheng et al., 2016a). Recent experimental evidence (Qiu et al., 2014) has shown that the Ti-6Al-2Sn-4Zr-2Mo (Ti-6242) alloy is dwell sensitive while Ti-6Al-2Sn-4Zr-6Mo (Ti-6246) is not at 20℃. Consistent crystal plasticity and DDP models used by Zheng et al. (2016b) found that the energy barrier for thermally activated dislocation escape from obstacles in alloy Ti-6246 is higher than that for Ti-6242 and demonstrated that the remarkably different stress dwell behaviours between the two alloys result from the differing time constants associated with the thermal activation process with respect to the dwell loading time. The dwell debit in aero-engine disc components is known empirically to be worst between temperatures of 90℃ and 120℃ (Zhang et al., 2015) for a number of commercially-useful Ti alloys, but not for others. Alloy Ti-6246, for example, is considered to show a low dwell debit at 20℃, but its dwell response at other temperatures has not been investigated.

Zhang et al. (2015) utilised crystal plasticity finite element modelling (CPFE) to address the temperature sensitivity of cold dwell fatigue in Ti-6Al alloys. Their results revealed that the maximum load shedding in these α-titanium alloys occurs at 120℃ and diminishes to zero at 230℃, for which the mechanistic basis was a changing rate sensitivity with temperature combined with the progressive decrease in slip strengths, noting that the rate of change of strength with temperature for $\langle a \rangle$-type slip differs from that of $\langle c + a \rangle$ slip. Ozturk et al. (2016) investigated the temperature sensitivity of alloy Ti-6242 also using CPFE and showed that the dwell effect in this alloy also diminishes with increasing temperature, but interestingly as a result only of the slip strength changes with temperature, therefore suggesting a subtly different mechanistic explanation to Zhang et al. (2015). The differences potentially originate from the veracity of the single crystal slip strength data utilised since these materials show strong strain rate sensitive behaviour (even at 20℃), but reported slip strengths are often not presented together with the strain rates at which the tests were carried out.

Dwell and no-dwell 10^4 cycle endurance fatigue tests carried out by Arthurs & Walker (reported by Zhang et al., 2015) on alloy Ti-829 found that the difference between the applied stresses respectively to give the same number of cycles to failure initially increased with temperature from 20℃ but peaked at a temperature of 120℃ and subsequently decreased and vanished at about 230℃. Zhang et al. (2015) showed that the predicted magnitude of the stress redistribution from soft to hard grain resulting from the dwell mirrored closely this temperature sensitivity. Spence et al. (2012) showed that the dwell debit in Ti-6246 is negligible and not influenced by temperature in the range of 20℃ to 150℃. Whittaker et al. (2010, 2013) revealed that Ti-6246 alloy displays a modest lifetime reduction between 450℃ and 550℃ under dwell loading in vacuum and the fatigue life is further reduced if the tests are carried out in air, but the mechanistic basis at these elevated temperatures, outside of those for which cold dwell is normally anticipated, remains unclear. Alloy Ti-6246 morphologies in service are often complex, comprising alpha-beta lath basket weave structures which may, in their own right, influence load shedding (Zhang et al., 2017). These complex morphologies are not addressed in this paper, but are the subject of future investigation. In aero-engine applications, the early take-off stage is key in the context of

dwell because of the interactions of high stress and transient temperature, which is initially low but quite quickly increases to a level higher than that critical for dwell. The transient, together with the critical dwell temperature and applied stress, therefore determine whether dwell fatigue is operative or not and hence understanding of the temperature sensitivity of dwell fatigue in relevant Ti alloys is crucial. The mechanistic basis of the temperature sensitivity and how the intrinsic material properties influence the dwell fatigue response have yet to be fully elucidated.

Hence, in this study, we aim to provide mechanistic explanations of the temperature sensitivity of dwell fatigue in two titanium alloys: Ti-6242 and Ti-6246. A 2D-DDP framework incorporating thermally activated dislocation escape together with slip transfer across grain boundaries is proposed to investigate the dwell fatigue behaviours between the temperatures of $-50℃$ and $390℃$. In the following sections, we briefly describe the DDP approach employed in this study, and firstly provide a quantitative investigation of the stress on the leading dislocations in a double pileup as a function of obstacle spacing and nucleation strength. We then study the temperature-dependent load shedding in the two aforementioned Ti alloys. Finally the differing dwell fatigue behaviours at various temperatures are categorised and the mechanistic basis of each category is discussed.

2. Discrete dislocation plasticity formulation

The classical two–dimensional discrete dislocation plasticity approach has been well described in earlier papers (Balint et al., 2005; Srinath and William, 2011; Van der Giessen and Needleman, 1995). Recent novel developments include the thermally activated escape of pinned dislocations from obstacles which is believed to be the key strain-rate sensitivity controlling mechanism in low strain rate regimes ($\leq 10^0 s^{-1}$) (Zheng et al., 2016c), and slip transfer through grain boundaries which is argued to be important in the dwell fatigue problem and can exacerbate the load shedding (Zheng et al., 2017). These two new implementations are included in the DDP model while grain boundary sliding is not considered in the present study because it is argued to be insignificant except for very small grain sizes (e.g. $< 100\text{nm}$) (Quek et al., 2016) or for high temperatures (e.g. $\geq 0.5T_m$) (Ahmed and Hartmaier, 2011) which are not directly related to the cold dwell fatigue problem. The DDP formulations are described in full in earlier papers (Li et al., 2009; Van der Giessen and Needleman, 1995; Zheng et al., 2016b-d), hence are only concisely summarised here.

The model is initially dislocation free but with Frank-Read sources and point obstacles randomly distributed with densities of ρ_{nuc} and ρ_{obs} respectively. A new dislocation dipole is generated once the shear stress on the source exceeds its strength τ_{nuc} for a period of time t_{nuc}. The source strengths are chosen from a normal distribution with mean strength $\bar{\tau}_{nuc}$ and 20% standard deviation. The nucleation time is inversely proportional to the shear stress τ as described by Agnihotri and Van der Giessen (2015)

$$t_{nuc} = \eta \frac{\phi}{\tau b} \tag{1}$$

where η is a material constant related to the viscous drag coefficient B, b is the magnitude of the Burgers vector and 2ϕ is the length of the Frank-Read source. The initial nucleation spacing L_{nuc} is taken such that the attraction stress between two opposite dislocations is equilibrated by the external applied stress when its value is equal to the source strength τ_{nuc}. The glide velocity of dislocations is governed by the linear mobility law as

$$v = \frac{\tau b}{B} \tag{2}$$

The motion of dislocations can be hindered by obstacles. Once a dislocation becomes pinned, it experiences a thermal activation process to overcome the obstacle and continue to glide along the slip plane. The frequency of successful jumps is given by Zheng et al. (2016c) as

$$\Gamma = \frac{\nu_D b}{l_{obs}} exp\left(-\frac{\Delta F}{kT}\right) sinh\left(\frac{\tau \Delta V}{kT}\right) \tag{3}$$

in which ν_D is the Debye frequency, l_{obs} the average obstacle spacing, thus the term $\nu_D b/l_{obs}$ is the frequency of attempts of dislocations to jump the energy barrier, successful or otherwise. Since the DDP model in the current study is two dimensional, the parameter l_{obs} actually represents the length of dislocation lines between obstacles in the out-of-plane direction. A constant value is used to minimize any contribution from 3D effects. Here the average obstacle spacing l_{obs} is chosen to be $2\mu m$ based on the random distribution of obstacles over the whole model sample. ΔF is the activation energy, k the Boltzmann constant, T the temperature and ΔV is the activation volume. Each obstacle is assigned a critical time t_{obs}, in a similar manner to the nucleation time t_{nuc}, in that once the dislocation has been pinned at the obstacle for longer than t_{obs}, it is freed from the obstacle. The time constant is defined as the inverse of the successful jump frequency, i.e. $t_{obs} = 1/\Gamma$.

After dislocations pass several obstacles, they may become trapped by a grain boundary. With further pileup in front of the GB, the stress acting on the lead dislocation increases and eventually it is able to transfer to another slip plane in the adjacent grain if the shear stress exceeds a threshold value τ_{pass}. The expression for the critical stress τ_{pass} is given by Li et al. (2009) as

$$\tau_{pass} b_1^2 = E_{gb}^t b_1 + \alpha G (\Delta b)^2 \tag{4}$$

where b_1 and Δb are the magnitudes of the Burgers vectors of incoming and residual dislocations at the GB respectively, $\alpha \approx 1$ is a material constant, G is the shear modulus and E_{gb}^t is the GB energy barrier per unit length for dislocation transmission (Sangid et al., 2011). Zheng et al. (2017) calculated the energy of symmetric and asymmetric tilt grain boundaries of titanium using atomistic simulations with the LAMMPS code (Plimpton, 2007). As the magnitude of residual dislocations at the boundary increases, so dislocation re-emission becomes possible and needs to be considered. Further details of the plane strain DDP formulation can be found in the literature, e.g. (Balint et al., 2005; Li et al., 2009; Zheng et al., 2016c, 2017).

Table 1. DDP model properties used unless stated otherwise.

G(MPa)	ν	b(nm)	ρ_{nuc} (μm^{-2})	ρ_{obs} (μm^{-2})	ΔV
29022	0.46	0.32	10	200	$0.5b^3$

B (Pa · s)	η (Pa · s)	ν_D (Hz)	k (JK^{-1})	ΔF (J/atom)	
				Ti − 6242	Ti − 6246
10^{-4}	90B	10^{11}	1.38×10^{-23}	9.8×10^{-20}	10.6×10^{-20}

The material properties and discrete dislocation modelling parameters for the two alloys Ti-6242 and Ti-6246 have been investigated and are given in Zheng et al. (2016b) at room temperature and are summarized in Table 1. The source and obstacle densities are chosen by calibration with the macroscopic rate sensitivity response from crystal plasticity modelling which in turn has been validated by successfully predicting the experimental test results of nano-indentation rate sensitivity measurements as detailed in Zheng et al. (2016b). Note that the dislocation mobility and thermally activated escape from obstacles employ the same properties in Table 1 for 1st order $\langle c+a \rangle$ type slip and $\langle a \rangle$ type systems. In fact, the dislocation population in the hard grain is two orders of magnitude lower than that in the soft grain for titanium alloys (Zheng et al. 2016a; Zheng et al. 2016b). Hence this assumption is reliable since the results are barely affected by the mobility and thermal activation processes in $\langle c+a \rangle$ systems. The source strength dependence on temperature, which is needed in the subsequent temperature-dependent analyses, is taken to be the same as that for the relevant slip system critical resolved shear stresses (CRSS) determined from experimental measurements (Williams et al., 2002) and crystal plasticity simulations in Ti-6Al alloys (Zhang et al., 2015). The same temperature dependence of the critical resolved shear stresses are also employed in the crystal plasticity studies of alloy Ti-6242 by Ozturk et al. (2016).

3. Dislocation distribution within double pileup

The process of dislocations escaping by thermal activation from pinned obstacles is argued to be the main mechanism controlling the rate sensitivity of titanium alloys for low strain rate regimes ($\sim 10^0 s^{-1}$) which is strongly associated with dwell fatigue in these alloys (Zheng et al., 2016c). When a number of dislocations on a given slip plane are forced against an obstacle under external stress, a dislocation pileup is formed and only the leading dislocation experiences the thermal activation process which enables it to overcome the obstacle and continue to glide along the slip plane. From equation (3), the two intrinsic properties controlling the successful jump frequency, i.e. the rate sensitivity of the material, are activation energy ΔF and activation volume ΔV, and even for the same material, the rate sensitivity is also strongly affected by the temperature T. The local stress states are argued to influence the sensitivity to these parameters significantly. In Stroh's crack nucleation model (Stroh, 1954), as well as subsequent models which consider alternative loading states (Bache, 2003; Zheng et al., 2016a), the stress on the fixed (leading) dislocation and the crack opening

stress are found to be related to the number of dislocations in the equilibrium pileup group. Hence the size of the dislocation pileup, the local stresses developed, and thermally activated dislocation escape are key in controlling load shedding and dwell fatigue sensitivity. Hence in this section, we calculate the size of a double pileup group from DDP simulations and compare results with a previous analytical solution, in order to demonstrate the important role of external stress in nucleation strength, argued to be crucial for the dwell fatigue problem normally associated with low stress loading.

Consider a Frank-Read source located on a slip plane with two inescapable obstacles sitting on the same plane either side of the source as shown in Fig. 2. The source is activated under the external stress and a double pileup is formed. The stress acting on the leading dislocation of each pileup group is τ_{dis}. The external stress τ_{ext} consists of the contribution from the applied loading and the stresses of all other dislocations. The size of each pileup between the source and the obstacle at the equilibrium state was estimated by Hirth and Lothe (1982) as

$$N = \frac{(1-\nu) l_{obs} \tau_{ext}}{Gb} \tag{5}$$

The analytical solution in equation (5) was obtained with the assumption that the stress is balanced everywhere on the slip plane except on the two leading dislocations. However this solution neglected to consider the threshold strength of the Frank-Read source, i.e. the nucleation strength τ_{nuc}. In fact, in general, the source is switched off much earlier than implied by equation (5) due to the back stress of the dislocation dipoles and the whole system reaches equilibrium even though the total stress on the nucleation site is not zero.

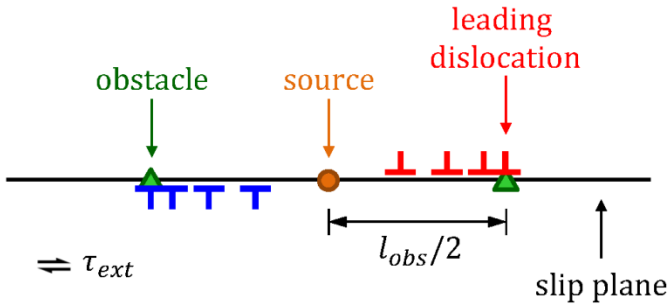


Fig. 2. Schematic of a double pileup which is formed from the activation of a Frank-Read source.

In order to obtain the number of dislocations in an equilibrium double pileup group with consideration of the Frank-Read nucleation strength, we perform the discrete dislocation simulation schematically shown in Fig. 2. We apply a constant shear stress of $\tau_{\text{ext}} = 500\text{MPa}$ to the entire system and assume the two obstacles have infinite strength. The source strength τ_{nuc} varies from 470 to 499MPa and the obstacle spacing l_{obs} from 0.4 to 2.0μm. For each nucleation strength and obstacle spacing, the system is computed until the stress on the leading dislocation reaches a stable value (determined from a threshold stress change $\leq 10^{-4}\text{MPa}$) and the size of each dislocation pileup group N is recorded. Fig. 3 compares the analytical solution to the DDP simulation results. The number of dislocations estimated by equation (5) is much larger than that determined from the DDP prediction. The size of the pileup increases with increasing obstacle spacing which is in accordance with the analytical

result. However, it also increases with decreasing nucleation strength, or in other words, with increasing external stress to nucleation strength ratio. The same result as in Fig. 3a can be achieved from the DDP analysis by reducing the nucleation strength to zero or much smaller compared to the external stress. However, cold dwell fatigue is a phenomenon which is observed to occur in components under relatively low stress levels, and in these circumstances, it is important to ensure that the source strength effect is properly considered. From the DDP simulations, the shear stress on the leading dislocation is calculated for each system at equilibrium as shown in Fig. 4. Similar to the size of dislocation pileup in Fig. 3b, the stress on the leading dislocation increases with increasing obstacle spacing or decreasing nucleation strength. Note that the stress increases by about 500MPa when a new dipole is generated.

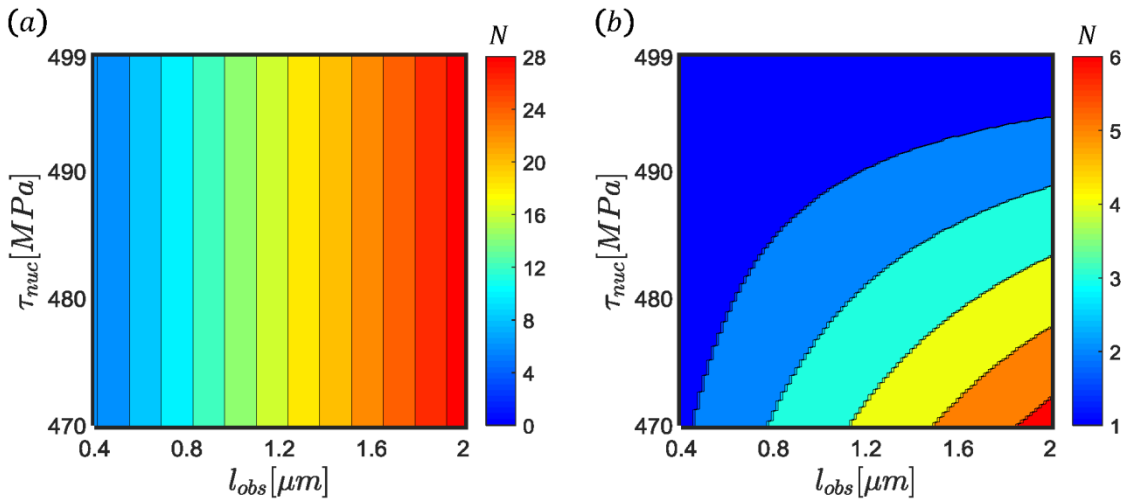


Fig. 3. Number of dislocations in each pileup group at equilibrium: (a) analytical solution in equation (5) and (b) results from DDP simulations

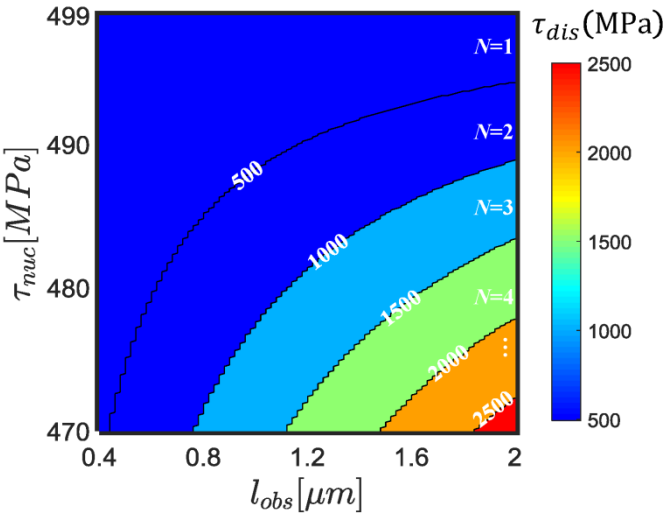


Fig. 4. Stress on the leading dislocation of a double pileup group from the DDP calculations.

4. Temperature-dependent load shedding in two titanium alloys

It is well-known that alloy Ti-6242 shows a significant dwell debit but that Ti-6246 does not at 20℃ (Jun et al., 2016; Kirane and Ghosh, 2008; Qiu et al., 2014; Spence et al., 2012; Zheng et al., 2016c). There is also evidence that the dwell sensitivity of alloy Ti-6242 increases to a peak at about 120℃ and subsequently diminishes at higher temperatures (Lütjering and Williams, 2003; Sinha et al., 2004), vanishing at 230℃ (Zhang et al., 2015). We focus in this section on the temperature-dependent load shedding in the well-known soft-hard grain combination embedded within oligocrystals of Ti-6242 and Ti-6246 alloys in order to assess the mechanistic basis and the differences which occur in the two alloys. Fig. 5 shows the loading, oligocrystal arrangement, boundary conditions and hard-soft grain regions of interest. As shown in Fig. 5c, a controlled Poisson Voronoi tessellation has been used to generate the crystal morphology using the VGRAIN software system (Zhu et al., 2014). The average grain size is $5\mu m^2$, minimum and maximum sizes are $3\mu m^2$ and $7\mu m^2$ respectively and the regularity parameter is 0.95. A soft-hard grain combination is located in the central region of the polycrystal for which the corresponding crystallographic orientations are shown in Fig. 5c. The surrounding grains are chosen to be randomly oriented but relatively well-oriented for slip. The model oligocrystal is subjected to uniaxial tension along the y-direction with the left and bottom surfaces constrained. Two loading conditions as illustrated in Fig. 5a and Fig. 5b are considered: (1) displacement-controlled loading up to 2% strain in 12s giving a total strain rate of $1.67 \times 10^{-3} s^{-1}$; (2) stress-controlled loading in which the imposed stress is increased at a constant rate to 0.95 of the yield stress $\sigma_{0.2}$ in 12s and then held at the maximum stress magnitude $0.95\sigma_{0.2}$ for a further 12s. The yy-stresses along the path $\mathrm{A}-\mathrm{A}'$ through the rogue grain combination before and after the stress dwell period are recorded. For the hard grain, the yy-stresses equate to those normal to the basal plane, considered key to driving quasi-cleavage facet nucleation in dwell, and hence important to consider in this study. In order to minimize the statistical effect due to the position chosen for the $\mathrm{A}-\mathrm{A}'$ path, an average of the yy-stresses along 20 paths which are all parallel to $\mathrm{A}-\mathrm{A}'$ and between the upper and lower bounds, as shown in Fig. 5d, is assessed to represent the stress through the two grains.

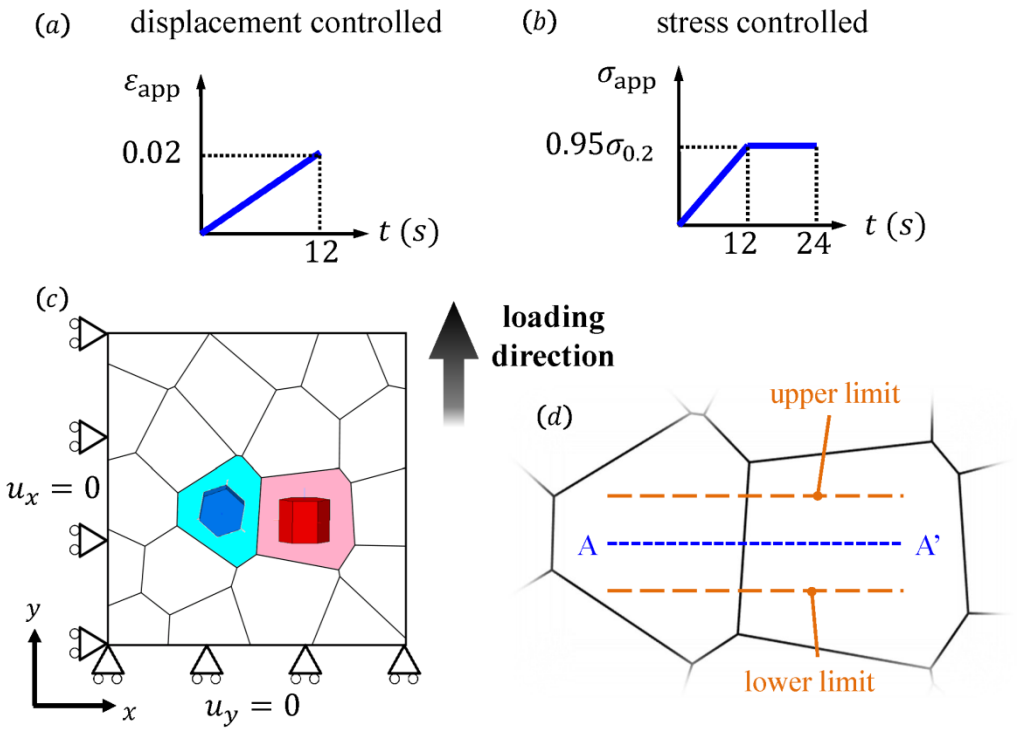


Fig. 5. Polycrystalline DDP model of two Ti alloys (a) displacement-controlled loading; (b) dwell stress controlled loading; (c) sample morphology generated from Voronoi tessellation and the imposed boundary conditions; (d) positions of A – A' path within the soft-hard grains.

Zhang et al. (2015) reported the temperature dependence of the critical resolved shear stresses for $\langle a \rangle$ and $\langle c+a \rangle$ type slip systems for Ti-6Al alloys, which were obtained from the experimental measurements of Williams et al. (2002). The latter measurements provide the sensitivity of CRSSs to temperature, and we utilise the same *temperature sensitivity* here in order to determine the temperature dependence of Frank-Read source strength. Zheng et al. (2016b) chose 480MPa and 560MPa as the mean strengths of Frank-Read sources on prismatic slip systems for alloys Ti-6242 and Ti-6246 respectively at 20℃. They have shown that using these values the DDP model shows good representation of the polycrystal stress-strain behaviour obtained from their CP model which in turn was calibrated against the experimental data of Qiu et al. (2014). The DDP model also successfully reproduced the experimentally measured low cycle dwell fatigue strain accumulation in Ti-6242 and Ti-6246 alloys at 20℃ (Qiu et al., 2014). Hence in the present study, the mean values of prismatic source strengths employed at 20℃ for Ti-6242 and Ti-6246 alloys are the same as those of Zheng et al. (2016b), with a temperature dependence obtained from Williams et al. (2002). The source strength of basal slip systems is taken to be the same as that of prismatic systems, but for the 1st order $\langle c+a \rangle$ pyramidal systems, source strengths are chosen to be three times higher than those for $\langle a \rangle$ type systems on the basis of the single crystal micro-cantilever bending measurements of Gong and Wilkinson (2009). The temperature dependencies of prismatic system source strengths in alloys Ti-6242 and Ti-6246 are therefore given by

$$\bar{\tau}_{nuc}^{Ti6242} = 0.0009T^2 - 0.5942T + 491.52 \quad (6)$$

$$\bar{\tau}_{nuc}^{Ti6246} = 0.0009T^2 - 0.5942T + 571.52 \quad (7)$$

where T is the temperature (℃). Both quantities are plotted in Fig. 6 together with prism critical resolved shear stress taken from Zhang et al. (2015) in order to demonstrate the same temperature *sensitivity*. The normal distributions of the sources from selected model samples are plotted in Fig.7. It can be seen that the overall shape of the histograms is similar but the peak probability is shifted to a higher range with increasing mean source strength. The weakest sources are about 180MPa lower than the mean value and the population of these sources is very low, e.g. less than 0.1%.

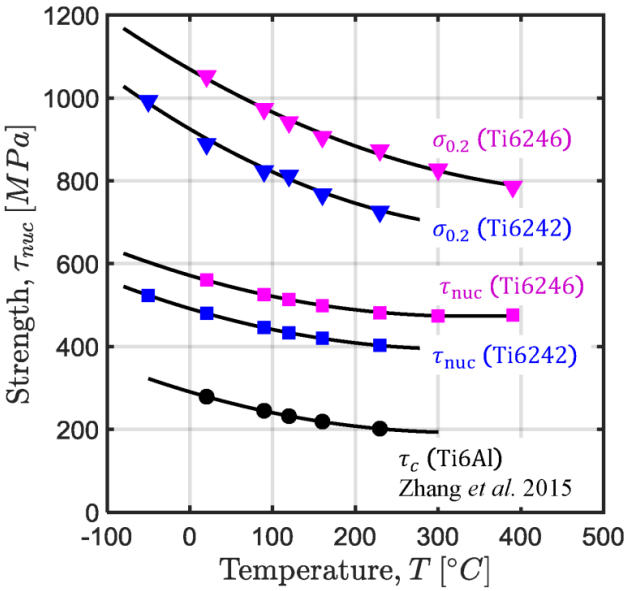


Fig. 6. Temperature-dependent nucleation strength of two alloys and the corresponding 0.2% yield strength extracted from DPP modelling of uniaxial displacement-controlled tension tests.

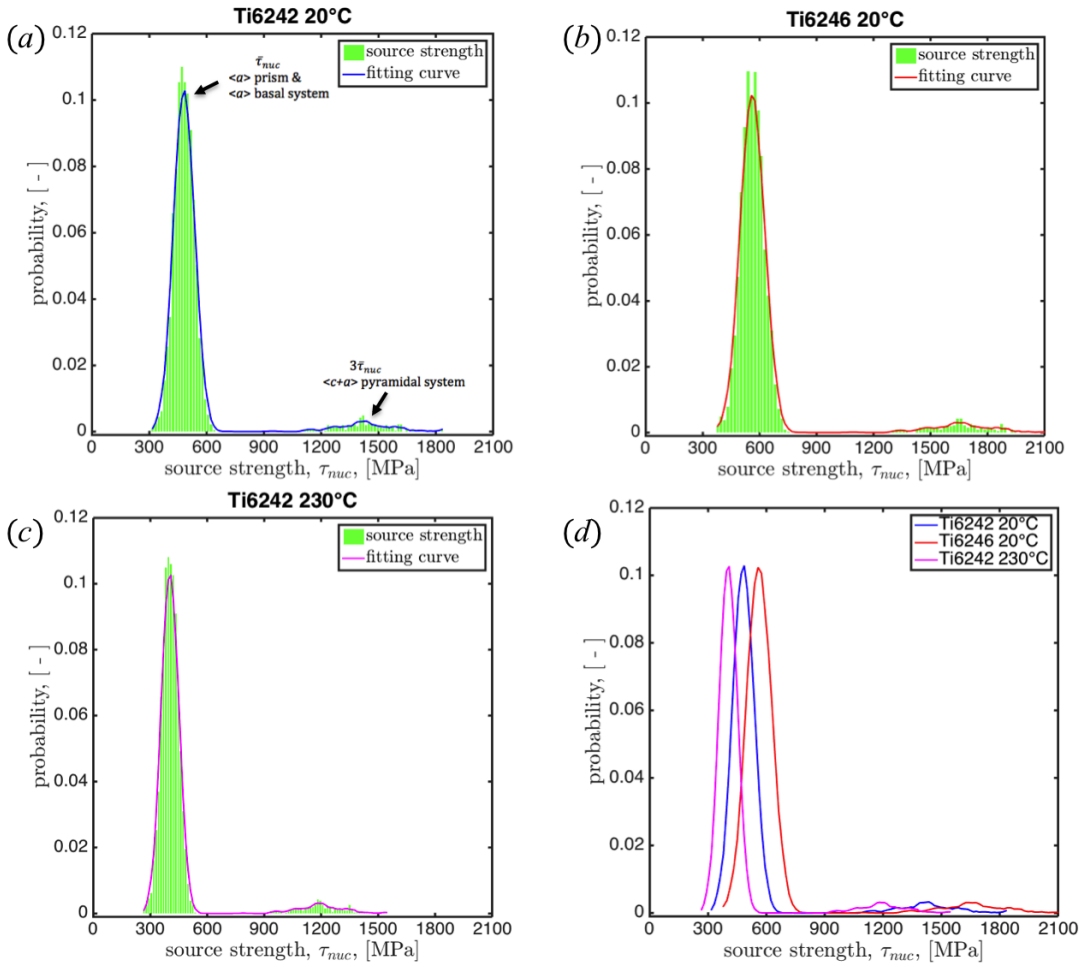


Fig. 7. Normal distribution of Frank-Read source strengths in (a) Ti-6242 alloy at 20℃; (b) Ti-6246 alloy at 20 ℃ and (c) Ti-6242 alloy at 230 ℃. Comparison of the fitting curves in (a)-(c) are summarised in (d).

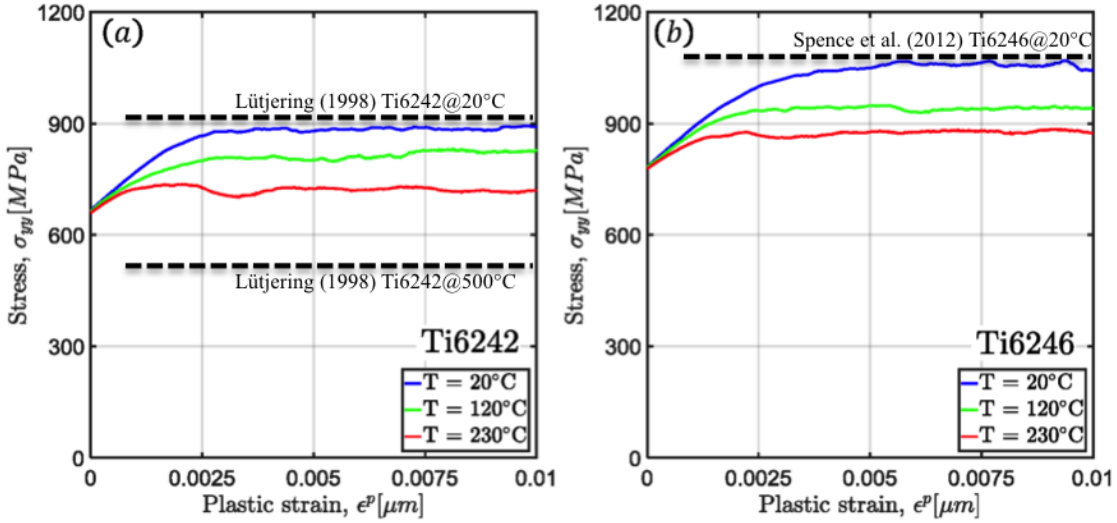


Fig. 8. DDP predicted stress responses of (a) Ti-6242 and (b) Ti-6246 under displacement-controlled loading at selected temperatures.

Displacement-controlled loading is imposed on the polycrystal model as shown in Fig. 5 for the two titanium alloys at a range of temperatures, and the resulting DDP predicted flow stresses versus plastic strains are shown in Fig. 8 for the three temperatures shown. Higher flow stresses for alloy Ti-6246 are obtained as anticipated showing good agreement with the experimental tensile tests by Lütjering (1998) and Spence et al. (2012). The flow stresses for the two alloys shown in Fig. 8 are extracted from the stress-strain curves by averaging the DDP polycrystal stress predictions, and simple fits to the data provide the following temperature sensitivities of yield stress.

$$\sigma_{0.2}^{Ti6242} = 0.0014T^2 - 1.1753T + 924.93 \quad (8)$$

$$\sigma_{0.2}^{Ti6246} = 0.0011T^2 - 1.1463T + 1069.2 \quad (9)$$

The two alloys are then investigated under conditions of stress-controlled loading as shown in Fig. 5b at a range of temperatures of interest. The maximum applied stress loading in all cases is chosen to be 0.95 of the flow strength as given by equation (8) and (9) for a given temperature. This is important in the context of dwell fatigue in order to provide consistency and comparison from alloy to alloy over the range of temperatures, by ensuring that the dwell stress applied is always $0.95\sigma_{0.2}$ at the temperature of interest. The resulting DDP predicted yy-stresses along the path $A - A'$ before and after the stress hold dwell period are shown in Fig. 9 for the two alloys for three temperatures of interest. In the hard grain, shown in Fig. 9, the yy-stress is in fact the crystal basal stress. The resulting yy-stress at the grain boundary for alloy Ti-6242 at 20℃ increases from 900MPa to about 1400MPa resulting from the strong load shedding from the adjacent soft grain to the hard grain during the stress dwell. The stress redistribution in this alloy is clearly very significant during dwell. However, the peak stress at the soft-hard grain boundary in Ti-6242 increases by about 750MPa to ~1600MPa during the dwell period at 120℃, which is very significantly higher than that at room temperature. The dwell debit associated with commercial titanium alloys in aero-engine discs is known to be worst at a temperature of about 120℃ (Zhang et al., 2015). The yy-stress distributions with the dislocation structure superimposed at the temperatures of 20℃, 120℃ and 230℃ are shown in Fig. 10. The dislocation structures before the stress hold are similar to one another at 20℃ and 120℃ but much more dislocation activity at the hold end is observed at 120℃, which leads to a more localised stress distribution in the hard grain, such that the load shedding is stronger. Note that the stress contours are shown between the limits of $\sigma_{app} - 300$MPa to $\sigma_{app} + 300$MPa for direct comparison, where σ_{app} is the applied stress. Returning to Fig. 9e, the yy-stresses in alloy Ti-6242 at a temperature of 230℃ are found to barely change during the stress dwell, showing that the load shedding which occurs from soft to hard grain has diminished away almost completely at this temperature in this alloy, suggesting that any dwell debit is also expected to diminish away. Correspondingly in Fig. 10e, the stress concentration at the soft-hard grain boundary is observed before the stress hold begins and remains stable during the holding period. The DDP predictions presented here for alloy Ti-6242 show good agreement with the crystal

plasticity analyses of Ti-6Al alloys by Zhang et al. (2015), confirming that the temperature-sensitive load shedding captured by the CP approach was accurate, even without the explicit representation of the detailed discrete dislocation activity that is achievable with the DDP methodology.

In order to assess the amount of load shedding that occurs before the stress hold begins, i.e. during the 12-second stress ramp time, the yy-stresses along the path $\mathrm{A}-\mathrm{A}'$ without change to material properties other than the specification of infinite activation energy ΔF are also plotted in Fig. 9. The stresses for infinite ΔF are found to be similar to those at the beginning of the stress hold with the original ΔF at 20℃ and 120℃ but much lower at 230℃, which suggests that most of the dislocation escape and hence load shedding occurs during stress dwell at low temperatures, while at high temperatures, dislocation escape occurs much more significantly during the stress ramp period.

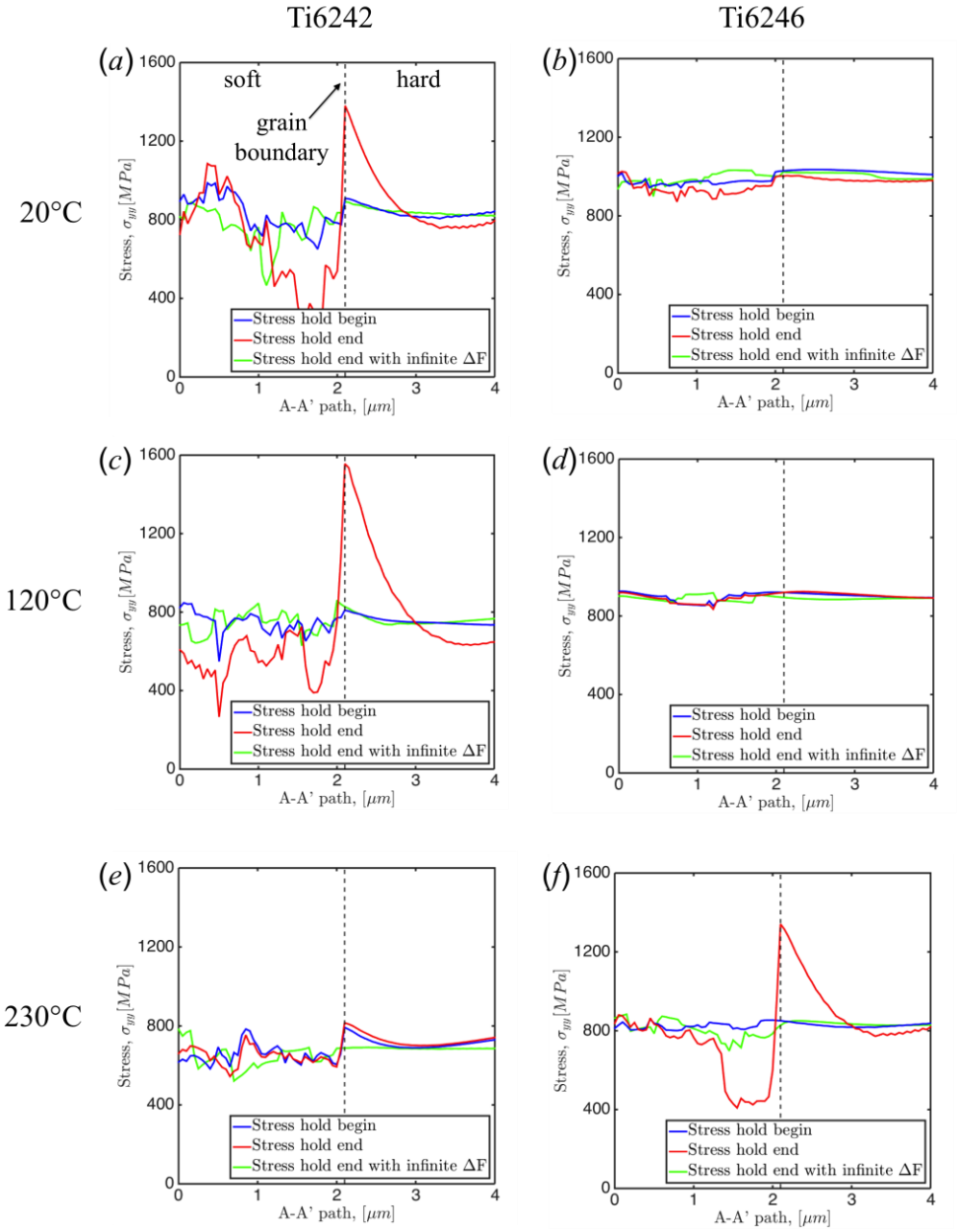


Fig. 9. yy-stress along A – A' path for increasing temperatures (a-b) 20℃, (c-d) 120℃, (e-f) 230℃.

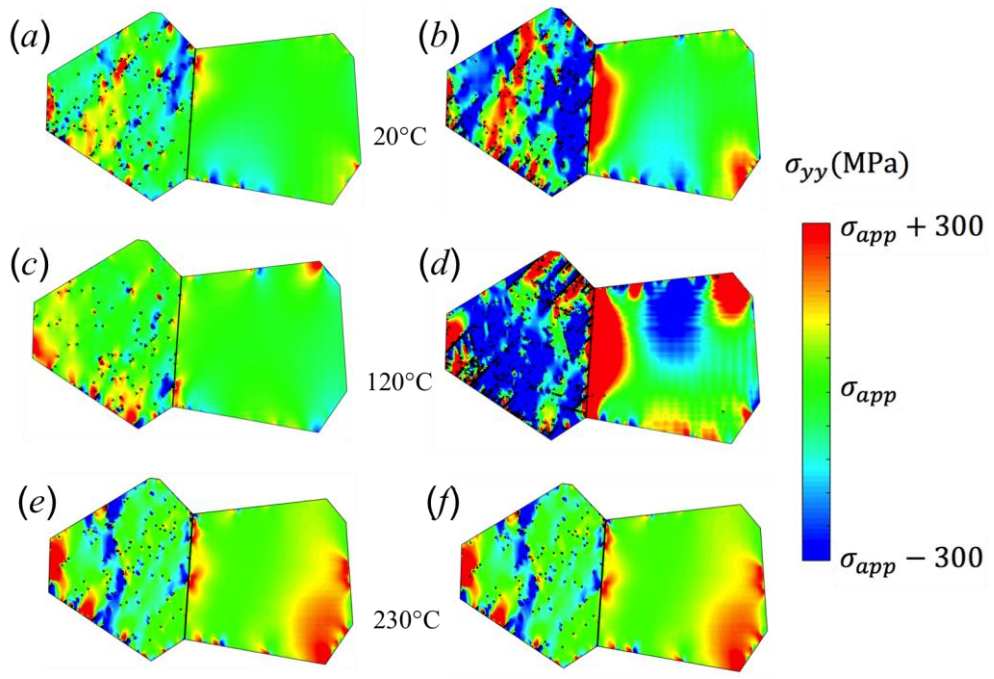


Fig. 10. Stress contours with the dislocation structure superposed before and after stress dwell of Ti-6242 alloy at (a/b) 20℃, (c/d) 120℃ and (e/f) 230℃.

Considering now the results for alloy Ti-6246 in Fig. 11, the stresses within the soft and hard grains in this alloy at 20℃ and 120℃ are more homogeneous compared to those for Ti-6242 and there is no obvious stress redistribution, or load shedding, observed during the stress hold for either temperature, quite unlike the behaviour observed for alloy Ti-6242. Experimental evidence also suggests that the dwell fatigue life of Ti-6246 alloy is not influenced by the dwell period in the temperature range of 20℃ to 150℃ (Spence et al., 2012). However, the DDP predictions indicate that stress redistribution, that is load shedding, from the soft to the hard grain during the stress dwell does occur at 230℃ in this alloy, as shown in Fig. 11f. This is similar to the load shedding observed in Ti-6242 but at significantly lower temperatures. By comparing with the stress distribution for an infinite ΔF, it is clear that most of the stress redistribution occurs during the dwell period. Further increases in temperature in alloy Ti-6246 show the DDP predicted load shedding increases further at a temperature of 300℃, and then diminishes at 390℃, as shown in Fig. 11a and b. There remains a GB stress increase of ~100MPa at 390℃ from the beginning to the end of the stress hold, but the dwell sensitivity is not examined at higher temperatures beyond 390℃ for which grain boundary sliding and dislocation absorption at the boundary must be accounted for in the polycrystal deformation mechanisms (Ahmed and Hartmaier, 2011; Quek et al., 2014). Interesting experimental observations provided by Whittaker et al. (2013), however, show that there is a small reduction (by a factor less than 1.5) in life under dwell loading for alloy Ti-6246 at 550℃, but the 'dwell debit' at such temperatures is argued to be dominated by environmental factors. The cycles to failure reduces by one order of magnitude if dwell is included when the tests are carried out in air. Hence, the load shedding in alloy Ti-6246 at high temperature, i.e.

$>$ 400℃, is negligible and any reduction in life which results under stress-hold loading originates from a different mechanistic basis in this alloy.

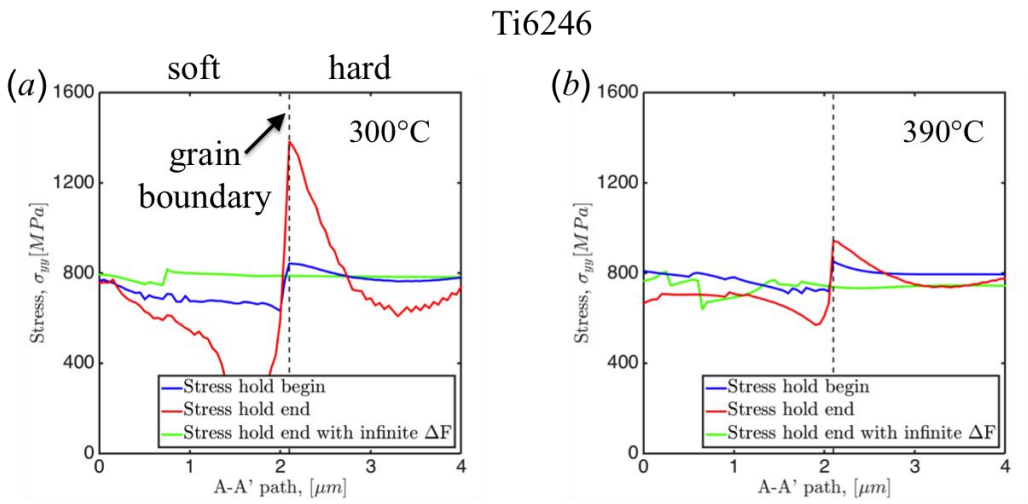


Fig. 11. yy-stress along A − A' path for Ti-6246 alloy at (a) 300℃ and (b) 390℃.

The magnitude of load shedding is directly related to the dislocation activity in the soft grain. The time-evolution of dislocation density in the soft grain during the loading history of the two alloys at selected temperatures is plotted in Fig. 12. At low temperatures, e.g. Ti-6242 at −50℃ and Ti-6246 at 120℃, the dislocation density is relatively low and is barely changed during the stress hold. This is because of the large time constant associated with thermally-activated dislocation escape and the fact that the back stresses introduced by the dislocation pile up in front of the obstacles switch off the activated Frank-Read sources, hence the overall dislocation activity is weak. At higher temperatures, e.g. Ti-6242 at 20℃ − 120℃ and Ti-6246 at 230℃ − 300℃, the dislocation densities are very similar before the stress hold but are significantly increased, by a factor of three to six, during the hold period. The dislocation escape time is similar in order of magnitude to the hold period, thus the pinned dislocations escape from the obstacles and more dislocations are nucleated from the sources. The escaped dislocations eventually pile up in front of the grain boundary and cause stress concentrations. With further increases in the temperature, e.g. for Ti-6242 at 230℃ and Ti-6246 at 390℃, the number of generated dislocations is larger than that for the low temperatures but smaller than for the intermediate temperatures. Most of the dislocations are nucleated before the stress dwell and very few new dislocations are generated during the hold period. At high temperatures, the time constant associated with dislocation escape is smaller hence the ratio of applied stress to nucleation strength, $0.95\sigma_{0.2}/\tau_{nuc}$, is also smaller compared to those at low temperatures. After dislocations quickly escape from obstacles, they pile up at the grain boundaries, and the back stresses from the pile-up groups switch off the sources, thus the dislocation population is not as large as the most dwell-sensitive temperature.

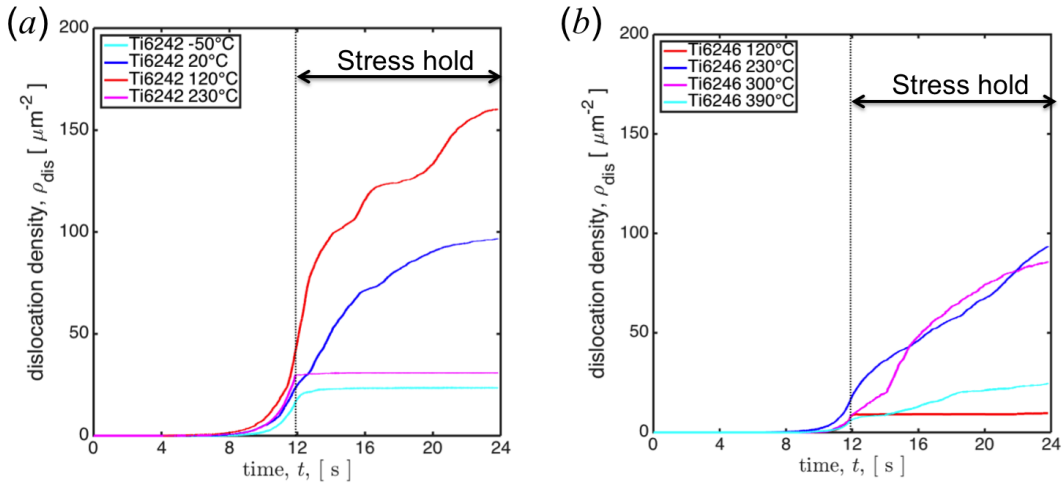


Fig. 12. The dislocation density development of (a) Ti-6242 and (b) Ti-6246 alloys at selected temperatures.

In order to assess the effect of dislocation activity in the soft grain on the magnitude of load shedding, a similar simulation to that for Ti-6242 alloy at 230℃ but with higher external applied stress, i.e. $\sigma_{app} = 1.05\sigma_{0.2}$, is carried out. In this case, the effect of the ratio of applied stress to nucleation strength is removed. The dislocation density development in the soft grain for applied stress $1.05\sigma_{0.2}$ at 230℃ is compared with those for an applied load of $0.95\sigma_{0.2}$ at 20℃ and 230℃ and results are plotted in Fig. 13. With higher applied stress, the Frank-Read sources nucleate more dislocations before being switched off by the back stress development. Hence the size of pile-ups at the obstacles and the dislocation density established before dwell are larger compared to low stress. However, since the obstacle escape time at 230℃ in Ti-6242 alloy is extremely low (almost zero) even for $0.95\sigma_{0.2}$ applied stress, increasing pile-up size has little observable effect on dislocation density during the dwell. Hence the equilibrium state is achieved during the load up, similar to that for low applied stress. From Fig. 13, the overall dislocation density in the soft grain at the end of loading under high applied stress at 230℃ is close to that obtained for 20℃, but in the former, almost all of the dislocation density has developed during stress load up and barely changes during the stress hold.

Hence the primary effect of increasing stress in Ti-6242 alloy at 230℃ is to lead to larger pile-ups at the soft-hard grain boundaries. The relationship between dislocation density developed and the stress redistribution during dwell is investigated in Fig. 14. Consider first the case of the difference in peak stress in dwell arising from inclusion of thermally activated dislocation escape compared to infinite activation energy (i.e. no dislocation escape) shown in Fig. 14a. Here, the peak stress difference after dwell is found to be almost linearly related to the final dislocation density. However, Fig. 14b shows the true load shedding during stress hold and at 230℃, a high applied stress allows more dislocations to accumulate at grain boundaries but this process is accomplished even before the stress hold begins due to the small time constant. Hence the magnitude of load shedding during the dwell period at this temperature transpires to be negligible, as is the case for low applied stress, despite the high dislocation density after load up.

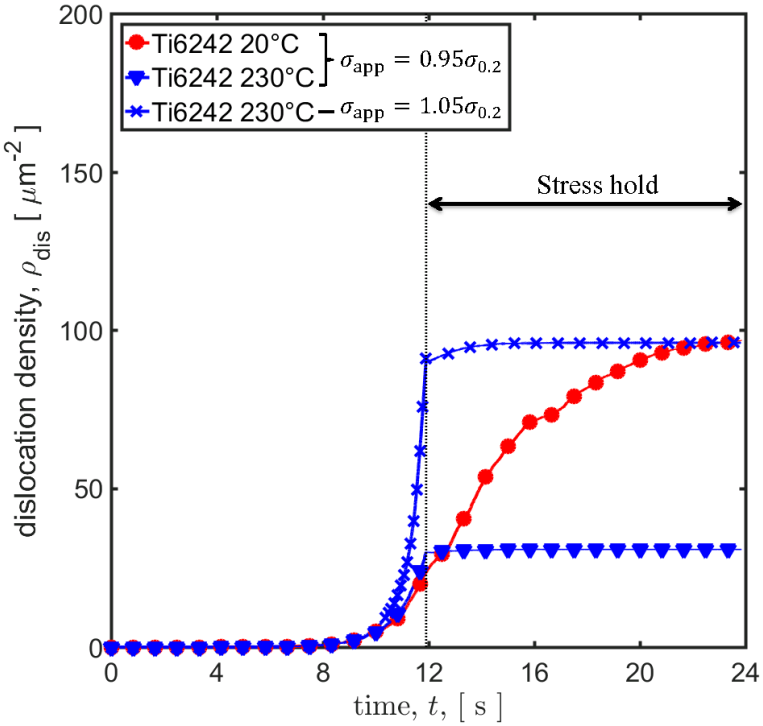


Fig. 13. The effect of external applied stress on the evolution of dislocation density in the soft grain.

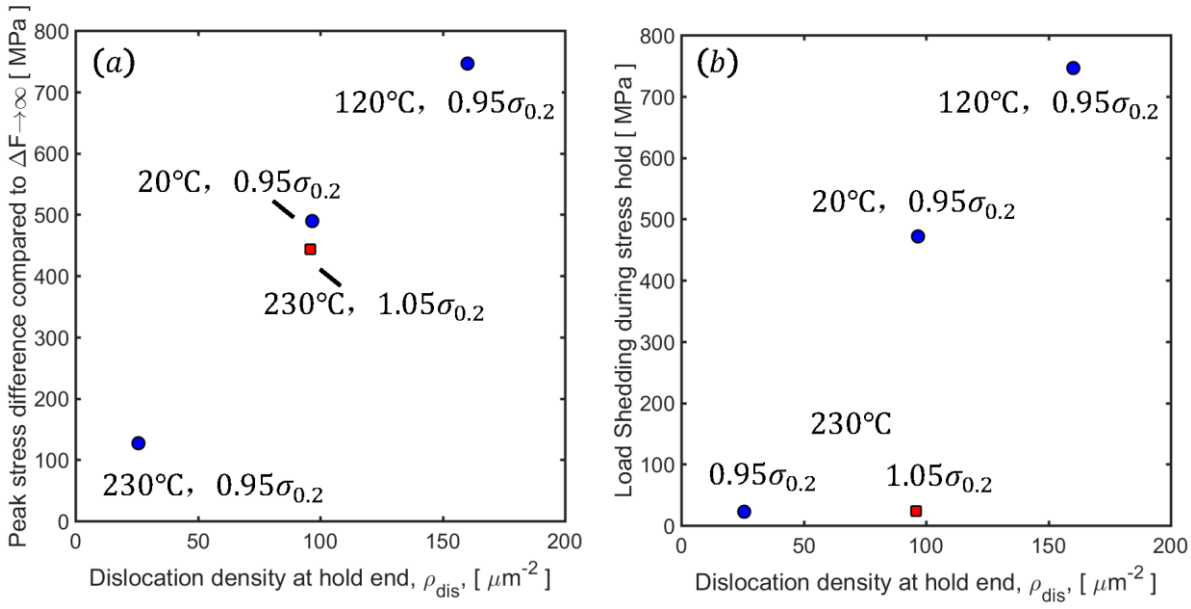


Fig. 14. (a) Peak stress difference at the soft-hard grain boundary for dwell resulting from thermally activated dislocation escape allowed and where activation energy is infinite ($\Delta F \to \infty$; no thermally activated escape) and (b) load shedding during stress dwell.

The predicted stress redistributions, or load shedding, which occur during stress dwell for the two Ti alloys considered across temperatures of interest are summarised in Fig. 15, from which the dwell-sensitive temperatures of alloy Ti-6246 are observed to be shifted to a higher range compared to that for Ti-6242. Typically, for alloy Ti-6246, the temperature range for which load shedding occurs is outside that relevant to normal operation and, it is argued,

explains why a dwell facet fatigue deficit has not been observed for this alloy in service (or laboratory testing) (Qiu et al., 2014). However, for alloy Ti-6242, the dwell-sensitive temperature range very much includes that relevant to in-service conditions, and for this reason, dwell fatigue is a very significant concern in this alloy. Five simulations with different source structures are carried out for alloy Ti-6242 at 120℃, which gives the highest load shedding among the temperatures of interest, to examine the stability of the data, and the error bar is displayed in Fig. 15. The variation of the stress redistributions due to the stochastic nature of DDP is found to be less than 80MPa.

A detailed assessment of the mechanistic basis at the dislocation level for the temperature sensitivity observed is presented in a later section, but we note that the activation energy for dislocation escape for alloy Ti-6246 (from Table 1) is higher than that for Ti-6242. The thermally activated dislocation escape time is given by equation (3) so that since alloy Ti-6246 has the higher activation energy barrier, higher temperatures than for Ti-6242 are necessary in order to achieve the same successful dislocation jump frequency or time to escape, to develop dwell sensitivity.

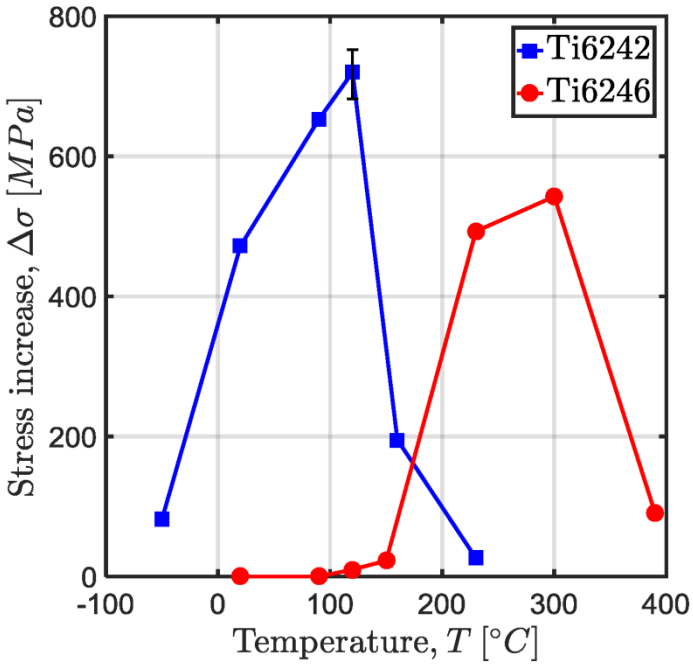


Fig. 15. Peak stress changing during the dwell period with temperatures.

For a given material, the obstacle time (i.e. time for dislocation escape) t_{obs} is a function of the temperature T and the stress on the leading dislocation of each pileup group τ_{dis}. Fig. 16a and Fig. 16b show contour distributions of the obstacle time in terms of temperature and leading pile-up dislocation stress for Ti-6242 and Ti-6246 respectively. Note that the lower and upper time limits of the contour plots are set to 10^{-1}s and 10^{3}s such that within these figures, if the obstacle time exceeds the upper limit (10^{3}s), then pinned dislocations are not able to escape during the in-service stress hold period so that no stress redistribution is expected. On the other hand, if the escape time is shorter than the lower limit (10^{-1}s) shown, the time of dislocations pinned at the obstacles is too short such that an equilibrium state is

established before the stress hold begins, so that no load shedding can be observed. As a result, only dislocations located in the colour range within Fig. 16a and Fig. 16b contribute to the dwell sensitivity of the alloys. The stresses on the leading pile-up dislocations which experience the thermal activation process are monitored during the loading history and plotted correspondingly in Fig. 16 for the temperatures shown. The lengths of the solid black lines in Fig. 16 reflect the range of stresses at leading pile-up dislocations predicted to occur for a given temperature. The lengths of the lines therefore indicate the range of pile-up stresses observed. Importantly, if the lines traverse the dislocation escape time range between 1 – 100s, this indicates that there is a strong propensity for load shedding to be observed in the specified alloy at the given temperature; conversely, if not, load shedding, and hence dwell debit, is not anticipated. The distribution of shear stresses acting on leading pile-up dislocations in alloy Ti-6242 at 20℃ and 120℃ is found to be broad and ranges from less than 100MPa to ~3000MPa, such that the escape time of some dislocations is comparable with the dwell time, indicating stress redistribution is both possible and likely. Furthermore, the range of dwell-eligible stresses at 120℃ is broader than that at 20℃ and as shown in Fig. 9 and Fig. 10, at both temperatures, Ti-6242 alloy displays significant load shedding but it is stronger at 120℃. At 230℃, however, the leading pile-up stresses of most pinned dislocations make the escape time at least two orders of magnitude shorter than the dwell period, hence these dislocations escape with ease so that no dwell load shedding is anticipated. On the contrary, for alloy Ti-6246 as shown in Fig. 16b, the dislocation stresses at 20℃ are too low for dislocation escape, hence there is no stress redistribution during the dwell and the soft-hard grain boundary stresses remain largely the same before and after dwell. At 120℃, there are some dislocations located in the colour area between 10^2s to 10^3s, but the dwell period in the DDP simulations is 12s, hence no dislocation is able to escape and no stress redistribution is observed. With further analysis, the majority of dislocations in alloy Ti-6246 at 120℃ are at the stresses lower than 700MPa which are out of the colour region. The very few dislocations which escape from obstacles within 10^3s are not able to induce significant load shedding. As for high temperatures, e.g. 230℃ and 300℃ for Ti-6246 the dwell-eligible stresses are low, but the range of pile-up stresses does include this range such that the associated dislocation escape times are similar to the dwell period and, as a result, strong load shedding is observed. As the temperature increases up to about 390℃, however, the dwell-eligible stresses are very low (less than 100MPa), hence the dislocations escape rapidly such that the material ceases to be sensitive to the dwell loading.

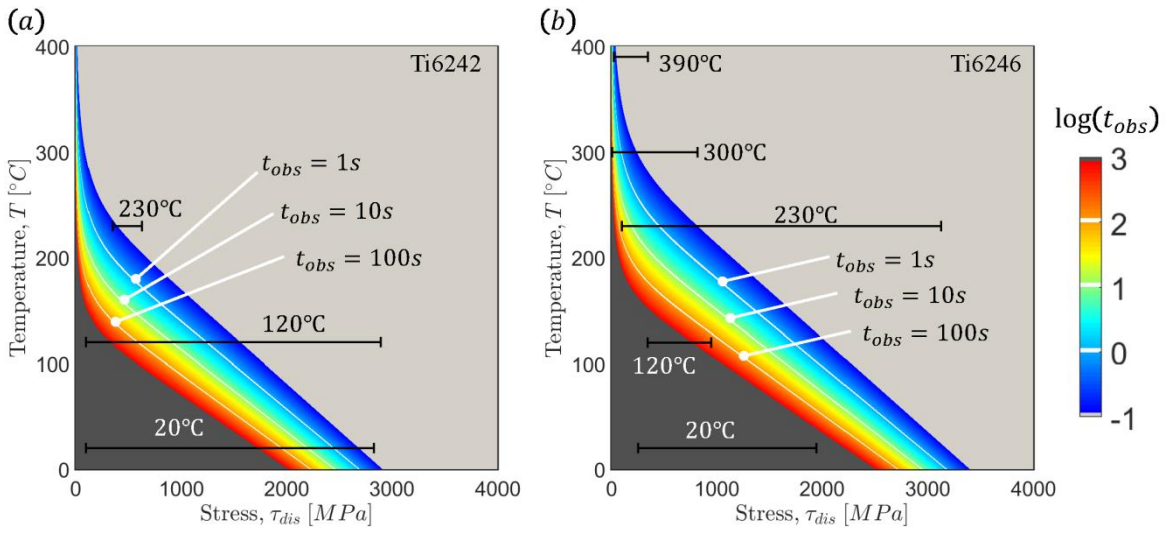


Fig. 16. Contours show the obstacle (dislocation escape) time as a function of temperature and dislocation stresses calculated from equation (3). The solid black lines indicate the DDP-calculated range of leading pile-up dislocation stress for the temperatures shown during the loading history.

An interesting observation is that for the cases of alloy Ti-6246 at 20℃ and alloy Ti-6242 at 230℃, no obvious load shedding is found in either, but the mechanisms are quite different. The plastic shear strain, defined as $\zeta = \sum_{m=1}^{3}|\gamma^m|$ where γ^m is the resolved shear strain on slip system m (Balint et al., 2005), is plotted in Fig. 17 for both cases after the dwell loading. As discussed in the previous section, the dislocation escape time associated with Ti-6246 alloy at low temperature is high such that the dislocations are not able to escape from the pinned obstacles. Hence several slip bands are observed to form in the soft grain but none of them is strong and the slip terminates at the location of obstacles. The activation energy of Ti-6242 is lower and when the temperature is high, the obstacle barrier to the dislocation motion is weak, hence multiple strong slip bands are formed as shown in Fig. 17b. Since the dislocations can easily jump the obstacles and pile up at the boundary before the dwell begins, the material maintains an equilibrium state during the stress hold, hence the peak stress at the GB does not increase and there is no load shedding

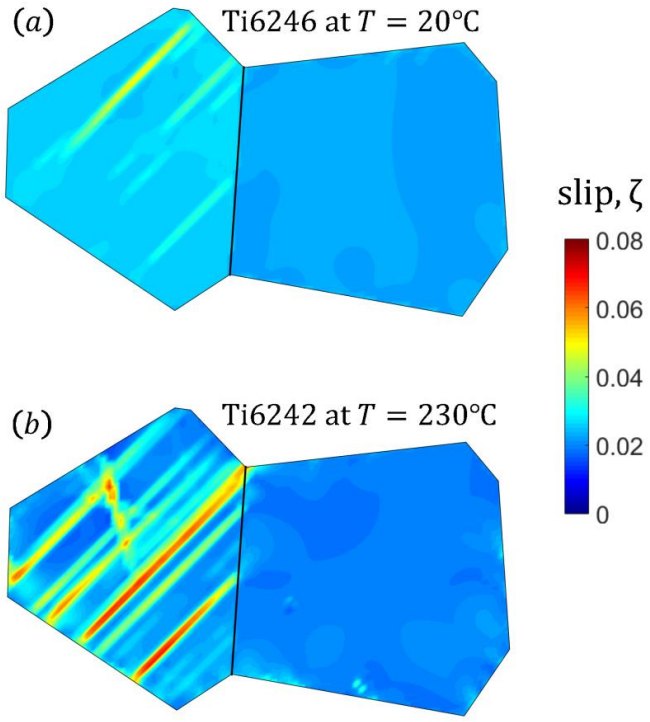


Fig. 17. Slip contours after dwell loading of (a) Ti-6246 alloy at 20℃ and (b) Ti-6242 alloy at 230℃; for both cases, no stress redistribution (load shedding) is observed.

5. Dislocation mechanisms in load shedding

Analysing the load shedding behaviours of alloys Ti-6242 and Ti-6246 over a range of temperatures allows the identification of three categories of deformation mechanisms under dwell fatigue loading: (1) obstacles behave as strong barriers to dislocation motion, and there is no load shedding; (2) resistance to dislocation glide from the obstacles is weak, and there is no load shedding; (3) dislocation-obstacle interaction is intermediate and the time constant associated with thermally activated escape is comparable to the dwell period, and there is strong load shedding. We analyse each of these categories in the following sections.

5.1. Obstacles behave as strong barriers to dislocation motion

This deformation mechanism is associated with low temperatures and for Ti alloys with high thermal activation energy. The obstacles are sufficiently strong in impeding dislocation escape and glide such that the time constant associated with thermal activation is much longer than the dwell period, hence once the dislocations are pinned at the obstacles, they are likely to remain in this state. An example of this process is for alloy Ti-6246 at low temperatures (< 150℃). As indicated in Fig. 18, dislocations become pinned but cannot escape through thermal activation within the dwell period. The stress redistribution within the soft and hard grains during dwell is negligible and no load shedding is expected, hence the material does not show any dwell debit. The stress distribution is found to be homogeneous compared to other categories. Since the dislocations cannot overcome the obstacles, the development of pile-up back stress switches off the dislocation sources rapidly, so this category of

deformation is associated with low dislocation populations especially around the grain boundaries. The slip bands developed are found to be terminated at the obstacles but not at the GBs as shown in Fig. 17a.

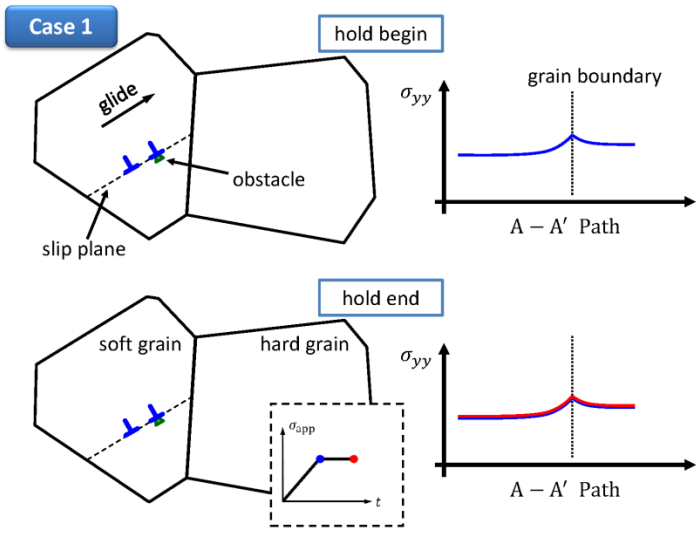


Fig. 18. Schematic for case 1 (low temperature or high activation energy): obstacles are strong and no load shedding occurs.

5.2. Weak resistance to dislocation glide from the obstacles

The dislocation-obstacle interactions in this category are very weak. It is associated with high temperatures and low activation energies. Dislocations become pinned at the obstacles but escape rapidly and continue to glide along the slip plane. The average dislocation velocity is much higher compared to Case 1. This type of interaction is always found at higher temperature in the Ti alloys and examples are alloy Ti-6242 at 230℃ and Ti-6246 at a temperature higher than 400℃. The obstacle resistance to dislocation glide is very weak and as a result, dislocations easily reach the grain boundaries. Much dislocation nucleation and slip occurs, uninhibited by obstacles, thereby reducing back stress development and so not diminishing nucleation leads to strong slip bands as shown in Fig. 17b. The thermal activation in this case takes place so rapidly that the material attains an equilibrium state before the stress hold begins. The soft-hard grain boundary stress is found to be moderate and no significant stress redistribution, or load shedding, occurs during the dwell, as illustrated schematically in Fig. 19. The alloys do not show dwell sensitivity under these conditions.

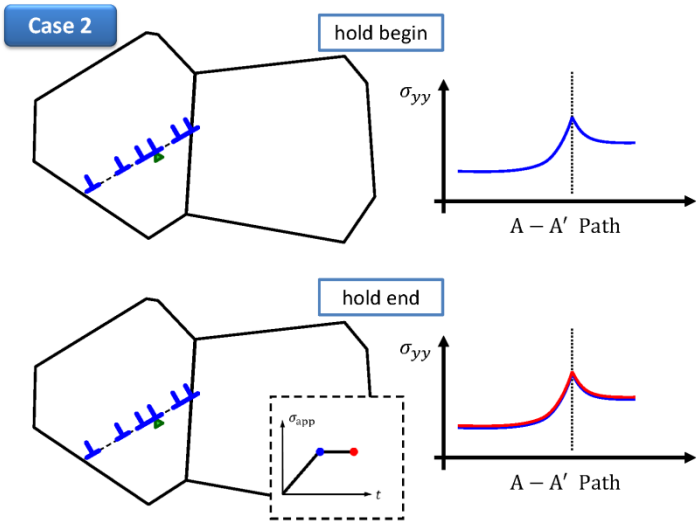


Fig. 19. Schematic for case 2 (high temperature or low activation energy): obstacles are weak and no load shedding occurs.

5.3. Dislocation-obstacle interaction is intermediate

If the time constant associated with thermal activation is similar to the stress dwell period, the process of dislocations becoming pinned at obstacles and subsequently escaping by thermal activation occurs potentially both before the stress dwell begins and also during the dwell. Dislocations which escape from obstacles by thermal activation encourage further nucleation (in that pile-up back stresses on the source are inhibited). The released dislocations glide eventually to reach the grain boundaries leading to the significant increase in stresses locally, during the stress dwell, as shown schematically in Fig. 20. Strong load shedding is expected under dwell fatigue loading together with a high dwell debit. Two examples of this category of deformation are that for alloy Ti-6242 at 20℃ and for Ti-6246 at 300℃. The dislocation-grain boundary interactions, together with the high basal stresses developed in the hard grain, are argued to be important to the facet crack nucleation (Bache, 2003; Stroh, 1954; Zheng et al., 2016a).

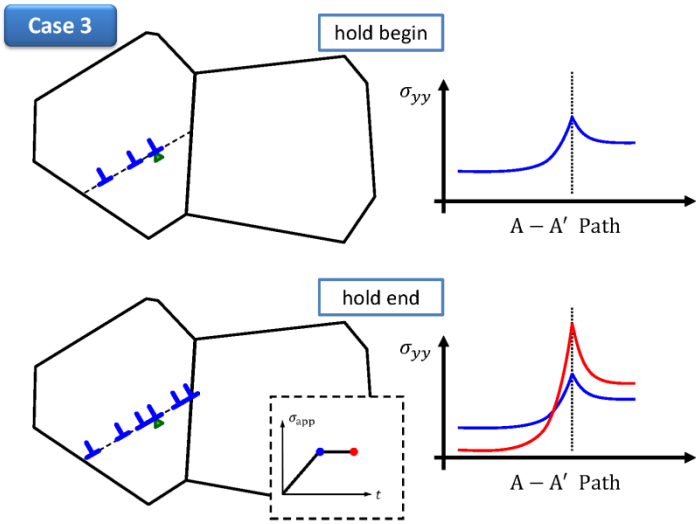


Fig. 20. Schematic for case 3 (temperature and activation energy are such that the time constant associated with thermally activated dislocation escape is similar to the time associated with the dwell loading): dislocation-obstacle interaction is intermediate and strong load shedding occurs.

Each of the DDP analyses carried out may be categorised into one of the three deformation mechanism cases described above and the results are summarised in Table 2. Independent experimental evidence and observations from the literature are also provided for each temperature reported where available, to provide the context to the DDP results. Persuasive agreement is established for alloy Ti-6242 with independent observations. In addition, the DPP model explains the absence of experimentally observed dwell sensitivity in alloy Ti-6246 at temperatures below 150℃. Regrettably, there is very little data for dwell in alloy Ti-6246 for temperatures above about 150℃. The main reason for this is that its dwell debit within the temperature regime relevant to aero-engine operation is negligible; that is, it is a *good* alloy with strong resistance to dwell fatigue. In this paper, we sought a temperature regime which would potentially drive dwell sensitivity in Ti-6246. An important conclusion from the work is that the alloy Ti-6246 is not dwell sensitive within the range of aero-engine temperatures to which it is subjected. This is a positive result since it provides the underpinning understanding of why Ti-6242 does dwell and Ti-6246 does not in service. However, the limited data that are available for alloy Ti-6246 at higher temperature indicates that the mechanistic nature of failure changes to prefer that dominated by environmental factors, superseding any effect of load shedding.

Table 2. Categories of dwell fatigue behaviours at different temperatures.

	T(℃)	Load shedding from DDP	Mechanistic Category	Evidence from literature
Ti-6242	-50	weak	1	-
	20	strong	3	Qiu et al. (2014) (Exp.Ti-6242) Bache et al. (1997) (Exp. IMI824) Ozturk et al. (2016) (CPFE Ti-6242) Evans and Gostelow (1979) (Exp. IMI685)
	90	strong	3	Zhang et al. (2015) (CPFE Ti6Al); (Exp. Ti829)
	120	strong	3	Zhang et al. (2015) (CPFE Ti6Al); (Exp. Ti829) Ozturk et al. (2016) (CPFE Ti-6242)
	160	weak	3	Zhang et al. (2015) (CPFE Ti6Al); (Exp. Ti829)
	230	none	2	
Ti-6246	20	none	1	Qiu et al. (2014) (Exp.Ti-6246) Bache (2003) (Exp. Ti-6246) Spence et al. (2012) (Exp. Ti-6246)
	90	none	1	Spence et al. (2012) (Exp. Ti-6246)
	150	none	1	
	230	strong	3	No direct evidence. Beranger et al. (1993) measured LCF life of Ti-6246 between 20 to 500℃, Whittaker et al. (2010) reported a strong environmental influence on fatigue life of Ti-6246 from 80 to 550℃
	300	strong	3	
	390	weak	2	
	550	-	2	Whittaker et al. (2013) (Exp. Ti-6246 shows low dwell debit in vacuum, high dwell debit in air)

Both the Ti-6242 and Ti-6246 alloys have rather complex morphologies depending on processing conditions with alloy Ti-6242 having a globular structure with primary alpha grains together with columnar alpha-beta grains, generally with a low volume fraction of beta. Ti-6246, however, is more complex with a basket weave type morphology and higher volume fraction of beta. In the present paper, these strongly differing morphologies have been represented in an homogenised manner; that is, the single (alpha-beta) crystal activation energies for thermally activated dislocation escape have been obtained for the two alloys to give optimised polycrystal plasticity model representations of the experimentally observed plastic strain accumulations for low cycle fatigue (no dwell) and for low cycle dwell fatigue (full details may be found in the earlier paper by Zheng et al. 2016b). The activation energies so obtained for alloys Ti-6242 and Ti-6246 therefore represent the average or homogenised response of the single alpha-beta units respectively. As a consequence, the details of the discrete nature of slip penetration across alpha-beta interfaces in the two alloys are not captured but it is argued that the resultant ‘grain-level’ strain rate sensitivity is represented. For this reason, the activation energy for Ti-6246 is consequently higher than that for Ti-6242, as shown in Table 1, because the alpha-beta basket weave morphology in Ti-6246 effectively gives rise to less rate sensitivity than the Ti-6242 alloy. It is noted that other researchers have suggested from experimental studies that the dwell insensitivity of Ti-6246 may well originate from the alpha-beta structure and the higher volume fraction of beta (Bache et al. 2003; Spence et al. 2012; Whittaker et al. 2010)

Current on-going work is addressing explicitly the alpha-beta morphologies in the Ti-6242 and Ti-6246 alloys using both crystal plasticity and discrete dislocation analyses in which the alpha and beta phase morphologies and the slip transfer across interfaces are explicitly recognised. Recent crystal plasticity analyses show that the colony structures associated with Ti-6242 give rise to very different rate sensitivity, and in turn stress relaxation and load shedding, compared to Ti-6246 with the former showing a significantly stronger rate sensitivity and hence propensity for load shedding. Interestingly, the alpha Burger orientation relationship variants have also been found using crystal plasticity modelling studies to influence quite strongly the rate sensitive response of alloy Ti-6246. Hence it is argued that the origin of the differing load shedding behaviours observed in alloys Ti-6242 and Ti-6246 very much depends upon the alpha-beta structures and morphologies, and this remains an active research area.

6. Conclusions

A discrete dislocation model which explicitly includes thermally activated escape of pinned dislocations and slip transfer across grain boundaries has been presented and employed to investigate dwell fatigue temperature sensitivity in Ti-6242 and Ti-6246 alloys. The key conclusions are summarized as follows:

1. The DDP model was used to determine the equilibrium position of dislocations within a double pileup as a function of obstacle spacing and Frank-Read source strength. The stress of the leading pile-up dislocation experiencing a thermal activation event can be explicitly calculated. The stress is found to be affected not only by the average obstacle spacing, but is also strongly influenced by the source strength.

2. A polycrystalline DDP model has been developed and utilised to investigate the temperature sensitivity of dwell in Ti-6242 and Ti-6246 alloys. Ti-6242 alloy is shown to have worst-case dwell sensitivity (that is, leading to the development of highest grain boundary load shedding) at about $120℃$. As temperature decreases to $\leq -50℃$ or increases to $\geq 230℃$, the dwell sensitivity diminishes away.

3. Ti-6246 alloy also shows dwell sensitivity and load shedding, but at temperatures higher than 150℃ which are significantly in excess of those for Ti-6242 and are outside the range of relevance for in-service conditions.

4. The mechanistic basis of load shedding has been investigated, together with its temperature sensitivity. The key controlling factor in this modelling methodology is the time constant associated with thermally activated dislocation escape with respect to the time of the stress dwell.

   (a) Low temperature or high activation energy for dislocation escape is found to inhibit dwell sensitivity since dislocations become pinned, inhibiting nucleation, and dislocation escape cannot occur during the stress dwell.

(b) High temperature or low activation energy lead to rapid pinned dislocation escape even prior to the stress hold such that dislocation nucleation and glide are uninhibited and significant slip banding termination at grain boundaries is seen. However, dwell sensitivity and load shedding are inhibited.

(c) For combinations of temperature and activation energy which give a time constant associated with dislocation escape that is comparable to the duration of the stress dwell, then significant dwell sensitivity and load shedding are observed.

The findings are in good agreement with independent experimental observations.

Acknowledgments

ZZ/FPED acknowledge the financial support by the Engineering and Physical Sciences Research Council for funding through the HexMat programme grant EP/K034332/1 and the China Scholarship Council (CSC). FPED also gratefully acknowledges Royal Academy of Engineering/Rolls-Royce Research Chair funding.

References

Agnihotri, P.K., Van der Giessen, E., 2015. On the rate sensitivity in discrete dislocation plasticity. Mechanics of Materials 90, 37-46.

Ahmed, N., Hartmaier, A., 2011. Mechanisms of grain boundary softening and strain-rate sensitivity in deformation of ultrafine-grained metals at high temperatures. Acta Materialia 59, 4323-4334.

Anahid, M., Samal, M.K., Ghosh, S., 2011. Dwell fatigue crack nucleation model based on crystal plasticity finite element simulations of polycrystalline titanium alloys. Journal of the Mechanics and Physics of Solids 59, 2157-2176.

Bache, M.R., 2003. A review of dwell sensitive fatigue in titanium alloys: the role of microstructure, texture and operating conditions. International Journal of Fatigue 25, 1079-1087.

Bache, M.R., Cope, M., Davies, H.M., Evans, W.J., Harrison, G., 1997. Dwell sensitive fatigue in a near alpha titanium alloy at ambient temperature. International Journal of Fatigue 19, 83-88.

Balint, D.S., Deshpande, V.S., Needleman, A., Van der Giessen, E., 2005. Discrete dislocation plasticity analysis of crack-tip fields in polycrystalline materials. Philosophical Magazine 85, 3047-3071.

Beranger, A.S., Feaugas, X., Clavel, M., 1993. Low cycle fatigue behavior of an α + β titanium alloy: Ti-6246. Materials Science and Engineering: A 172, 31-41.

Dunne, F.P.E., 2014. Fatigue crack nucleation: Mechanistic modelling across the length scales. Current Opinion in Solid State and Materials Science 18, 170-179.

Dunne, F.P.E., Rugg, D., 2008. On the mechanisms of fatigue facet nucleation in titanium alloys. Fatigue & Fracture of Engineering Materials & Structures 31, 949-958.

Dunne, F.P.E., Walker, A., Rugg, D., 2007a. A systematic study of hcp crystal orientation and morphology effects in polycrystal deformation and fatigue. Proceedings of the Royal Society of London A: Mathematical, Physical and Engineering Sciences 463, 1467-1489.

Dunne, F.P.E., Rugg, D., Walker, A., 2007b. Lengthscale-dependent, elastically anisotropic, physically-based hcp crystal plasticity: Application to cold-dwell fatigue in Ti alloys. International Journal of Plasticity 23, 1061-1083.

Evans, W.J., Bache, M.R., 1994. Dwell-sensitive fatigue under biaxial loads in the near-alpha titanium alloy IMI685. International Journal of Fatigue 16, 443-452.

Evans, W.J., Gostelow, C.R., 1979. The effect of hold time on the fatigue properties of a β-processed titanium alloy. MTA 10, 1837-1846.

Gong, J., Wilkinson, A.J., 2009. Anisotropy in the plastic flow properties of single-crystal α titanium determined from micro-cantilever beams. Acta Materialia 57, 5693-5705.

Hasija, V., Ghosh, S., Mills, M.J., Joseph, D.S., 2003. Deformation and creep modeling in polycrystalline Ti–6Al alloys. Acta Materialia 51, 4533-4549.

Hirth, J.P., Lothe, J., 1982. Theory of dislocations.

Jun, T.-S., Armstrong, D.E.J., Britton, T.B., 2016. A nanoindentation investigation of local strain rate sensitivity in dual-phase Ti alloys. Journal of Alloys and Compounds 672, 282-291.

Kirane, K., Ghosh, S., 2008. A cold dwell fatigue crack nucleation criterion for polycrystalline Ti-6242 using grain-level crystal plasticity FE Model. International Journal of Fatigue 30, 2127-2139.

Kirane, K., Ghosh, S., Groeber, M., Bhattacharjee, A., 2009. Grain Level Dwell Fatigue Crack Nucleation Model for Ti Alloys Using Crystal Plasticity Finite Element Analysis. Journal of Engineering Materials and Technology 131, 021003-021003.

Li, Z., Hou, C., Huang, M., Ouyang, C., 2009. Strengthening mechanism in micro-polycrystals with penetrable grain boundaries by discrete dislocation dynamics simulation and Hall–Petch effect. Computational Materials Science 46, 1124-1134.
Lütjering, G., 1998. Influence of processing on microstructure and mechanical properties of $(\alpha + \beta)$ titanium alloys. Materials Science and Engineering: A 243, 32-45.
Lütjering, G., Williams, J.C., 2003. Titanium. Springer.
Ozturk, D., Shahba, A., Ghosh, S., 2016. Crystal plasticity FE study of the effect of thermo-mechanical loading on fatigue crack nucleation in titanium alloys. Fatigue & Fracture of Engineering Materials & Structures 39, 752-769.
Plimpton, S.J., 2007. LAMMPS: Large-scale Atomic/Molecular Massively Parallel Simulator. Sandia National Laboratories.
Qiu, J., Ma, Y., Lei, J., Liu, Y., Huang, A., Rugg, D., Yang, R., 2014. A Comparative Study on Dwell Fatigue of Ti-6Al-2Sn-4Zr-xMo (x = 2 to 6) Alloys on a Microstructure-Normalized Basis. Metall and Mat Trans A 45, 6075-6087.
Quek, S.S., Chooi, Z.H., Wu, Z., Zhang, Y.W., Srolovitz, D.J., 2016. The inverse hall–petch relation in nanocrystalline metals: A discrete dislocation dynamics analysis. Journal of the Mechanics and Physics of Solids 88, 252-266.
Quek, S.S., Wu, Z., Zhang, Y.W., Srolovitz, D.J., 2014. Polycrystal deformation in a discrete dislocation dynamics framework. Acta Materialia 75, 92-105.
Sangid, M.D., Ezaz, T., Sehitoglu, H., Robertson, I.M., 2011. Energy of slip transmission and nucleation at grain boundaries. Acta Materialia 59, 283-296.
Sinha, V., Mills, M.J., Williams, J.C., 2004. Understanding the contributions of normal-fatigue and static loading to the dwell fatigue in a near-alpha titanium alloy. Metall and Mat Trans A 35, 3141-3148.
Sinha, V., Mills, M.J., Williams, J.C., Spowart, J.E., 2006. Observations on the faceted initiation site in the dwell-fatigue tested ti-6242 alloy: Crystallographic orientation and size effects. Metall and Mat Trans A 37, 1507-1518.
Spence, S., Evans, W., Cope, M., 2012. Dwell fatigue on TI 6246 at near ambient temperatures, ICF 9-Sydney, Australia-1997.
Srinath, S.C., William, A.C., 2011. New algorithms for discrete dislocation modeling of fracture. Modelling and Simulation in Materials Science and Engineering 19, 045009.
Stroh, A.N., 1954. The Formation of Cracks as a Result of Plastic Flow. Proceedings of the Royal Society of London A: Mathematical, Physical and Engineering Sciences 223, 404-414.
Van der Giessen, E., Needleman, A., 1995. Discrete dislocation plasticity: a simple planar model. Modelling and Simulation in Materials Science and Engineering 3, 689.
Whittaker, M.T., Harrison, W., Hurley, P.J., Williams, S., 2010. Modelling the behaviour of titanium alloys at high temperature for gas turbine applications. Materials Science and Engineering: A 527, 4365-4372.
Whittaker, M.T., Evans, W., Harrison, W., 2013. Fracture mechanisms due to Fatigue, Creep and Environmental damage in titanium alloys, ICF12, Ottawa 2009.
Williams, J.C., Baggerly, R.G., Paton, N.E., 2002. Deformation behavior of HCP Ti-Al alloy single crystals. Metall and Mat Trans A 33, 837-850.
Zhang, Z, Dunne, F.P.E., 2017. Microstructural heterogeneity in rate-dependent plasticity of multiphase titanium alloys. Jnl. Mech. Phys. Solids, 103, 199–220.
Zhang, Z., Cuddihy, M.A., Dunne, F.P.E., 2015. On rate-dependent polycrystal deformation: the temperature sensitivity of cold dwell fatigue. Proceedings of the Royal Society of London A: Mathematical, Physical and Engineering Sciences, 471, 2181.
Zheng, Z., Balint, D.S., Dunne, F.P.E., 2016a. Discrete dislocation and crystal plasticity analyses of load shedding in polycrystalline titanium alloys. International Journal of Plasticity 87, 15-31.

Zheng, Z., Balint, D.S., Dunne, F.P.E., 2016b. Dwell fatigue in two Ti alloys: An integrated crystal plasticity and discrete dislocation study. Journal of the Mechanics and Physics of Solids 96, 411-427.
Zheng, Z., Balint, D.S., Dunne, F.P.E., 2016c. Rate sensitivity in discrete dislocation plasticity in hexagonal close-packed crystals. Acta Materialia 107, 17-26.
Zheng, Z., Balint, D.S., Dunne, F.P.E., 2017. Investigation of slip transfer across HCP grain boundaries with application to cold dwell facet fatigue. Acta Materialia 127, 43-53.
Zhu, H.X., Zhang, P., Balint, D., Thorpe, S.M., Elliott, J.A., Windle, A.H., Lin, J., 2014. The effects of regularity on the geometrical properties of Voronoi tessellations. Physica A: Statistical Mechanics and its Applications 406, 42-58.